Frequency-Domain Analysis of Strongly Nonlinear Circuits Using a Consistent Large-Signal Model

Tapani Närhi

Abstract—**This paper describes an analysis method that extends the applicability of the frequency-domain methods to strongly nonlinear circuits. Nonlinearities are described with Chebyshev expansions which are evaluated with a numerically stable three-term recurrence formula. The method is coupled with a novel, measurement-based consistent modeling approach which allows improved accuracy in describing the frequency-dependence of the measured small-signal parameters. The analysis method and the modeling approach are verified by comparing measurements and calculations on a MESFET mixer, driven with two and three tones.**

I. Introduction

HARMONIC-BALANCE (HB) methods have matured into a reliable workhorse in the design of nonlinear microwave circuits. However, when the circuit has several excitation frequencies, the analysis becomes easily impractical due to the long computation time. Even with only two independent tones, the analysis is very slow on a workstation [1], and the calculation of the intermodulation products of a mixer with three independent frequencies is most conveniently done on a supercomputer [2]. At present the maximum number of independent frequencies that can be handled with HB software is limited to three, although there would be need for more, for example in the satellite communication systems.

Frequency-domain methods do not suffer from the same limitations: both the linear and nonlinear parts of the circuit are analysed in the frequency domain so that the time-consuming conversions between frequency and time domains are avoided [3]. The number of independent frequencies is not limited to three; it is the total number of frequencies, not the number of fundamental frequencies, that determines the complexity of the problem. The spectral-balance method of Rhyne *et al.* [4], which uses power series to approximate the nonlinear functions, is a well-known example of frequency-domain methods.

Modeling of nonlinear devices has been the weakest point of the frequency-domain approach. Nonlinear components are traditionally modeled in the time domain by using algebraic equations to describe the nonlinearities. These equations themselves are typically simplified with nonconsistent construction, limited bias or frequency range, etc., and determining the model parameters by fitting the equations into measured data is often a complicated and inaccurate procedure. Such a model can be converted suitable for the frequency-domain analysis by fitting power series [4], polynomial expansions [5], or specific functional approximations [6] to the model equations. However, this is neither accurate nor elegant approach.

Second, approximation of strongly nonlinear functions with power series requires that there is a great number of terms, e.g., several tens, in the series. Large coefficients are needed for the high-degree terms in the power series and this degrades significantly the numerical accuracy. As a result, the application of the methods using power series to describe the nonlinearities has been limited to relatively weakly nonlinear circuits. For example, to the author's knowledge no results have been published about the application of the generalized power series method [4] to strongly nonlinear cases like mixers under large RF-signal excitation.

This paper describes a frequency-domain method where both the limitations of the conventional power series approach are removed: All the nonlinearities are represented in this method with Chebyshev expansions instead of power series [5], [7], and [8]. Excellent numerical stability of these expansions, when evaluated through a recurrence formula, allows the use of high-degree expansions, which are necessary for describing strongly nonlinear devices. A novel consistent modeling approach is presented, where the frequency-domain large-signal model is constructed directly from small-signal measurements through integration [9], without the intermediate step of fitting to algebraic model equations. In comparison, e.g., to the Root model [10], this approach offers possibilities for more accurate representation of the frequency-dependence of the small-signal y-parameters of the device. This principle allows the description of the frequency-dependent characteristics (e.g., g_{ds}) of the device in a natural way, in contrast to the HB methods, where the time-domain formulation of the nonlinearities makes it very difficult to construct a large-signal model that is accurate both at dc and RF. In fact, the earlier disadvantage of the frequency-domain approach, modeling of nonlinear devices, is now turned into an advantage.

Coupling the new large-signal model to the frequency-domain algorithm results in an effective and accurate method for analysing nonlinear circuits under multi-tone excitation. This is demonstrated in the last part of the paper, where measured and calculated results for a MESFET mixer are compared. The method is so efficient that the intermodulation

Manuscript received December 27, 1993, revised November 12, 1995

The author is with ESA-ESTEC, European Space Agency, 2200 AG Noordwijk, The Netherlands

Publisher Item Identifier S 0018-9480(96)01441-X.

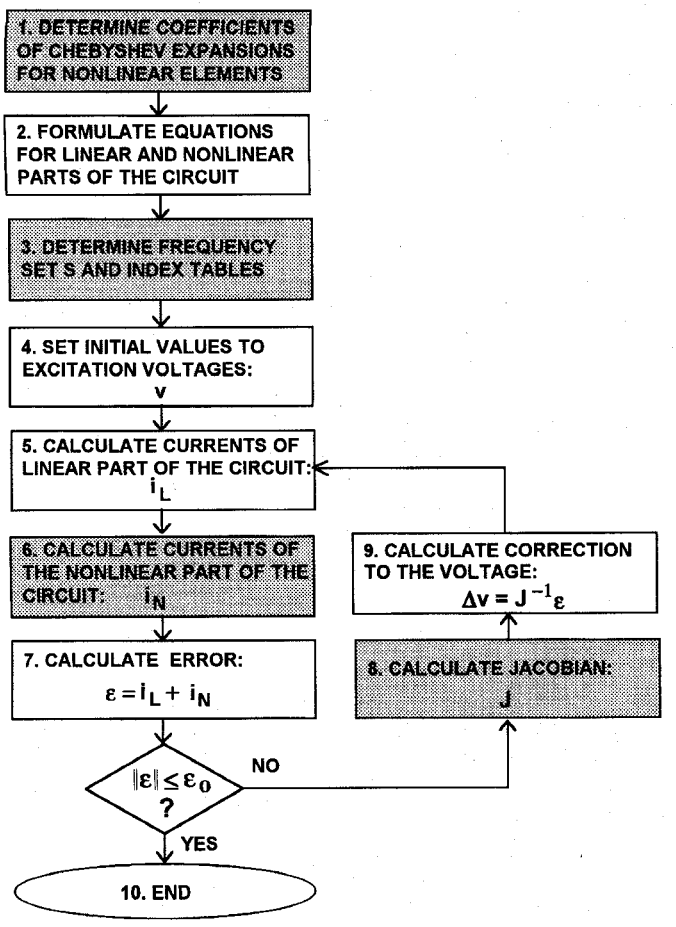

Fig. 1. Flow-chart of the frequency-domain algorithm.

analysis of the mixer, with three independent tones and over 100 frequencies in total, is possible on a PC, even with so high RF levels that the mixer is driven to the saturation of the IF and beyond.

II. Frequency-Domain Algorithm

The flow chart of the algorithm is shown in Fig. 1. Main differences in comparison to the conventional HB methods are in the following blocks.

1) Nonlinear elements are approximated with Chebyshev expansions (Step 1).
2) The frequency-domain response of the nonlinear elements for given spectra of the driving voltages is calculated directly in the frequency domain (Step 6). For this purpose the frequencies are selected prior to the analysis in Step 3.
3) The frequency-domain formulation of the problem allows very economical evaluation of the Jacobian in Step 8.

With strongly nonlinear circuits the full Newton step fails very often and some strategy for global convergence has to be adopted. Presently, the backtracking line-search algorithm is used for this purpose [11]. Details of the frequency-domain algorithm are discussed in the following chapters, followed by a description of the large-signal model.

A. Selection of Frequencies

In the frequency domain method of this study, the frequencies at which the circuit is to be analysed, are always selected before solving the circuit equations. During the analysis, this set of frequencies, or the *frequency set S*, is kept fixed and only those harmonics and intermodulation products falling on these frequencies are taken into account in the analysis. Each frequency ω_k of the frequency set can be written with the help of P *fundamental frequencies* $\omega_1, \omega_2, \cdots, \omega_P$

$$\omega_k = k_1\omega_1 + k_2\omega_2 + \cdots + k_P\omega_P \tag{1}$$

where the *harmonic numbers* $k_1, \cdots, k_P$ are integers. For each frequency the *order* is defined as

$$\mathrm{ORD}(\omega_k) = \sum_{i=1}^{P} |k_i| \tag{2}$$

Determining the frequencies includes the selection of the maximum values for the harmonic numbers $k_1, \cdots, k_P$, so that all the significant frequencies are retained, but the total number of frequencies *Nfreq* is kept to the minimum.

Two quantities are used to determine the frequency set, *maximum number of harmonics* (**maxH**) and *maximum order of intermodulation* (*maxIMt*). **maxH** is a vector containing the maximun harmonic numbers for each fundamental frequency

$$\mathbf{maxH} = [k_{1\max}\, k_{2\max} \cdots k_{P\max}]^T \tag{3}$$

and *maxIMt* is a scalar. **maxH** gives the maximum number of harmonics for each of the P fundamental frequencies and *maxIMt* indicates the maximum order of intermodulation products taken into account. Only positive frequencies are used in the calculations. Thus the frequency set S is defined by the following conditions

$$S = \{\omega \mid \omega = k_1\omega_1 + k_2\omega_2 + \cdots + k_P\omega_P; C1, C2, C3\} \tag{4}$$

$C1$. $\omega \ge 0$

$C2$. $|k_i| \le k_{i\max}, \quad i = 1, 2, \cdots, P$

$C3$. $\mathrm{ORD}(\omega) \le maxIMt$, when at least two harmonic numbers, k_i and k_j are not zero.

This selection of frequencies is unconventional. More often the spectrum is either *triangular*, for which $C3$ holds for all i, or *rectangular*, which is defined by $C2$. The reason for this more complicated truncation criteria is the additional flexibility in controlling the frequency set, as the number of harmonics for each of the fundamental frequencies can be separately controlled and, in addition, the maximum order of the intermodulation products can be independently defined.

In this study the frequencies of the frequency set are arranged, starting from zero (=dc) according to the increasing order. The highest order in the frequency set is *maxORD*

$$maxORD = \max\{k_{i\max}, maxIMt\}. \tag{5}$$

Within each order, the frequencies are sorted by magnitude, with the lowest frequency coming first and the highest frequency last. The frequencies are written, in this order, to

the frequency vector (frequency table) **ftab**. All the voltages, currents, charges etc are represented in the analysis with complex vectors of phasors with length equal to *Nfreq*, the number of frequencies. The phasors are arranged in the same order as in **ftab**, and if the frequency f_k of a certain phasor V_k is needed in the analysis, it is available as the kth element of the frequency table **ftab**$[k]$. Associated with the frequency table is the *intermodulation table* **imt**, which is a vector of integers giving the indices (row numbers) of **ftab** at which each IM-order begins. This vector is used when performing the multiplication of two waveforms in the frequency domain.

B. Frequency-Domain Operations

All the voltages, currents, charges and other waveforms of the nonlinear circuit are represented in the following form in the time domain, here written for the voltage

$$v(t) = \sum_{k=0}^{N} \{V_{kc} \cos(\omega_k t) - V_{ks} \sin(\omega_k t)\}. \tag{6}$$

Thus the frequency component of the voltage at frequency ω_k is given either with two real numbers, V_{kc} and V_{ks}, or with a complex *phasor* V_k. These two are related according to

$$V_k = |V_k| e^{j\varphi_k} = V_{kc} + jV_{ks}. \tag{7}$$

The time-domain quantities, *waveforms*, are written with lowercase letters, e.g., $v(t)$, and the corresponding representations in frequency domain, *(frequency) spectra*, are written with **bold** typeface, e.g., **v**.

Following symbolic notation is used to indicate the relationship between the time-domain and frequency-domain representations

$$\mathbf{v} = F\{v(t)\} \quad \text{or} \quad \mathbf{v} \leftrightarrow v(t). \tag{8}$$

The spectrum corresponding to the waveform (6) is given with the real $(2N+1) \times 1$ vector $\underline{\mathbf{v}}$, where underlining indicates the fact that it is a *real* vector

$$\underline{\mathbf{v}} = [V_0 \quad V_{1c} \quad V_{1s} \quad V_{2c} \quad V_{2s} \quad \cdots \quad V_{Nc} \quad V_{Ns}]^T. \tag{9}$$

Alternatively, the spectrum is given with the complex vector of phasors (V_0 is the real dc voltage)

$$\mathbf{v} = [V_0 \quad V_1 \quad V_2 \quad \cdots \quad V_N]^T. \tag{10}$$

Generally, lowercase letters are used for scalars, bold lowercase letters for vectors, and bold capital letters for matrices.

Nonlinear components are described in this work with the help of single and double Chebyshev expansions for the nonlinear functions. For strongly nonlinear devices also rational functions can be used [12]. Evaluation of the time-domain response of these components to an excitation of the form of (6) involves only the basic algebraic operations addition, subtraction, multiplication and division between the two waveforms $a(t)$ and $b(t)$. In the frequency-domain algorithm the response is calculated directly in the frequency domain. This means that we have to be able to calculate the frequency-domain equivalents to these basic operations between two frequency spectra **a** and **b**, remembering that **a** and **b** are complex vectors of the phasors like in (10), where the frequencies are truncated and sorted as was described earlier.

Addition and subtraction of two spectra are trivial

$$c(t) = a(t) \pm b(t) \quad \leftrightarrow \quad \mathbf{c} = \mathbf{a} \pm \mathbf{b}. \tag{11}$$

In contrast, time-domain multiplication and division are nonlinear operations resulting in the generation of new frequency components. Product in the time domain corresponds to the *convolution* in the frequency domain

$$c(t) = a(t) \cdot b(t) \quad \leftrightarrow \quad \mathbf{c} = \mathbf{a} * \mathbf{b} \tag{12}$$

and division in the time domain is the inverse operation, corresponding to the *deconvolution* in the frequency domain

$$b(t) = c(t)/a(t) \quad \leftrightarrow \quad \mathbf{b} = \mathbf{c} \# \mathbf{a}. \tag{13}$$

Here the symbol "#" is used to indicate the deconvolution. Repeated application of these operations during the evaluation of the response of the nonlinear component results in very large number of frequencies, even if there are only few driving frequencies. However, phasors at many of these frequencies are insignificant (harmonics and intermodulation products of high order). The basic principle is adopted that the frequencies of interest are determined *prior* to any circuit analysis. Thus the *length* of voltage, current, charge, etc., vectors remains constant (=*Nfreq*) throughout the analysis and only the complex amplitudes of each frequency component change during the analysis.

In the following chapters the calculation of the last two operations in the frequency domain is described, first two different ways of calculating the product (12) and then the division (13). These operations were outlined earlier in [12], and a similar set of operations was also included in the "arithmetic operator method" in [6]. However, since the approach taken here with special emphasis to the effective truncation of frequencies, is somewhat different to that in [6], it is justified to present a detailed description of the frequency-domain operations.

Direct Multiplication: The most straightforward way of calculating the time-domain product (12) is to multiply, in turn, each complex phasor $A_i = A_{ci} + jA_{si}$ of $a(t)$ by each phasor $B_j = B_{cj} + jB_{sj}$ of $b(t)$ and apply trigonometric rules to assign the result to the corresponding phasor $C_k = C_{ck} + jC_{sk}$ of $c(t)$. Three possible cases are encountered when multiplying phasors A_i and B_j, depending on the magnitudes of ω_i and ω_j

1) Sum frequency:
$$C_k = A_i \cdot B_j/2 \qquad \omega_k = \omega_i + \omega_j \in S$$

AND

{2) Difference frequency (positive):
$$C_k = A_i \cdot B_j^*/2 \qquad \omega_k = \omega_i - \omega_j \in S$$

OR

3) Difference frequency (negative):
$$C_k = A_i^* \cdot B_j/2 \qquad \omega_k = \omega_j - \omega_i \in S\}$$

where the asterisk (*) indicates complex conjugate.

Thus each phasor of **c** is calculated

$$C_k = C_{kp} + C_{kmp} + C_{kmn} \tag{14a}$$

where

$$C_{kp} = \frac{1}{2} \sum_{(i,j)\in I_p} A_i \cdot B_j \tag{14b}$$

$$C_{kmp} = \frac{1}{2} \sum_{(i,j)\in I_{mp}} A_i \cdot B_j^* \tag{14c}$$

$$C_{kmn} = \frac{1}{2} \sum_{(i,j)\in I_{mn}} A_i^* \cdot B_j \tag{14d}$$

and

$$I_p = \{(i,j) \mid \omega_i + \omega_j = \omega_k; \omega_i, \omega_j, \omega_k \in S\} \tag{14e}$$

$$I_{mp} = \{(i,j) \mid \omega_i - \omega_j = \omega_k; \omega_i, \omega_j, \omega_k \in S\} \tag{14f}$$

$$I_{mn} = \{(i,j) \mid \omega_j - \omega_i = \omega_k; \omega_i, \omega_j, \omega_k \in S\}. \tag{14g}$$

On some occasions, it is useful to be able to omit the multiplications between high-order phasors. Recalling that the frequencies in **a** and **b** are determined by the frequency table **ftab** (through quantities **maxH** and *maxIMt*), we now define a new quantity *maxIMp*, which sets the maximum order of the intermodulation products that are taken into account when calculating the convolution. Setting *maxIMp* = 2 *maxORD* is the normal case and it means that *all* the components falling on the frequency set S are taken into account when calculating the convolution, while *maxIMp* = 1 neglects all the frequency conversions. *maxIMp* gives additional flexibility, as the number of multiplications in the calculation of the convolution can be reduced by excluding products between high-order frequencies by setting *maxIMp* < 2 *maxORD*. This is demonstrated in Fig. 2.

The phasors in **a** and **b** are arranged in the ascending order of intermodulation and thus it is easy to avoid unnecessary multiplications by performing the multiplication of each A_i in turn with only those B_j with $0 \le j \le jmax$, where $jmax$ is the maximum index of **ftab** so that $\mathrm{ORD}(\omega_i) + \mathrm{ORD}(\omega_j) \le$ *maxIMp*. In the practical procedure it is important to avoid comparison and branching operations and to use predetermined, direct mapping instead. Since we have defined exactly in which order and how the multiplications are performed, the result from each product of two phasors can in fact be assigned to the corresponding output phasor C_k with the help of *precalculated* index vectors. All the necessary products (but only those!) between the real and imaginary parts of the phasors of the two spectra are calculated into a single vector and the final result is obtained simply through assignment and addition operations using these index vectors.

These two features, avoiding all unwanted multiplications and the use of precalculated index tables, are instrumental in making the convolution procedure efficient. This procedure of calculating the truncated convolution was originally used in [5] and is conceptually similar to the spectrum mapping principle of [13].

Convolution as a Matrix Product: The direct procedure described above is fast and well suited to repeated calculation of the product (12) as required in the recursive evaluation of the Chebyshev expansions in the frequency domain. In some occasions, however, it is advantageous to formulate the product as an explicit matrix product

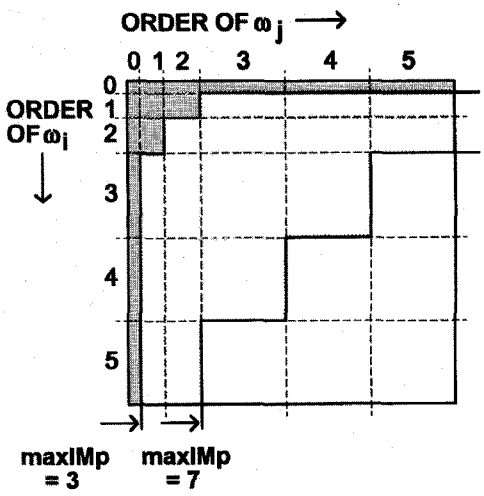

Fig. 2. Example on how the frequencies included in the frequency-domain convolution are affected by the parameter *maxIMp*. Two fundamental frequencies.

$$c(t) = a(t) \cdot b(t) \quad \leftrightarrow \quad \underline{\mathbf{c}} = \underline{\mathbf{A}} \cdot \underline{\mathbf{b}}. \tag{15}$$

This is the case for example when the inverse operation or division has to be performed, as will be seen later. Calculating the convolution as a matrix product was originally developed in [12], where rational functions were used to describe strongly nonlinear components. The arithmetic operator method of reference [13] follows the same principle.

The product (15) cannot be formulated using complex representation (10), instead $\underline{\mathbf{a}}$ and $\underline{\mathbf{b}}$ are written as real $(2N+1) \times 1$ vectors, as in (9). The $(2N+1) \times (2N+1)$ convolution matrix $\underline{\mathbf{A}}$ is formed through a transformation from $\underline{\mathbf{a}}$, here written symbolically with operator "$\sim$"

$$\underline{\mathbf{A}} = \tilde{\underline{\mathbf{a}}} \tag{16}$$

This transformation is found by first writing (15) in the matrix form

$$\begin{bmatrix} C_0 \\ C_{1c} \\ C_{1s} \\ \vdots \\ C_{ic} \\ C_{is} \\ \vdots \\ C_{Nc} \\ C_{Ns} \end{bmatrix} = \underbrace{\begin{bmatrix} \cdot & \cdot & \cdot & \cdot & \cdot & \cdot & \cdot & \cdot & \cdot \\ \cdot & \cdot & \cdot & \cdot & \cdot & \cdot & \cdot & \cdot & \cdot \\ \cdot & \cdot & \cdot & \cdot & \cdot & \cdot & \cdot & \cdot & \cdot \\ \cdot & \cdot & \cdot & \cdot & \cdot & \cdot & \cdot & \cdot & \cdot \\ \cdot & \cdot & \cdot & \cdot & Z_{cc}^{(ij)} & Z_{cs}^{(ij)} & \cdot & \cdot & \cdot \\ \cdot & \cdot & \cdot & \cdot & Z_{sc}^{(ij)} & Z_{ss}^{(ij)} & \cdot & \cdot & \cdot \\ \cdot & \cdot & \cdot & \cdot & \cdot & \cdot & \cdot & \cdot & \cdot \\ \cdot & \cdot & \cdot & \cdot & \cdot & \cdot & \cdot & \cdot & \cdot \\ \cdot & \cdot & \cdot & \cdot & \cdot & \cdot & \cdot & \cdot & \cdot \end{bmatrix}}_{\underline{A}(f)} \cdot \begin{bmatrix} B_0 \\ B_{1c} \\ B_{1s} \\ \vdots \\ B_{jc} \\ B_{js} \\ \vdots \\ B_{Nc} \\ B_{Ns} \end{bmatrix}. \tag{17}$$

Submatrix $Z^{(ij)}$ gives the contribution of the frequency component at ω_j in $b(t)$ to the frequency ω_i in $c(t)$

$$\begin{bmatrix} C_{ic} \\ C_{is} \end{bmatrix} = \sum_{j=0}^{N} \begin{bmatrix} Z_{cc}^{(ij)} & Z_{cs}^{(ij)} \\ Z_{sc}^{(ij)} & Z_{ss}^{(ij)} \end{bmatrix} \cdot \begin{bmatrix} B_{jc} \\ B_{js} \end{bmatrix} = \sum_{j=0}^{N} Z^{(ij)} \begin{bmatrix} B_{jc} \\ B_{js} \end{bmatrix}. \tag{18}$$

It is calculated, for each pair of frequencies ω_i and ω_j, from those phasors A_k in $a(t)$ which, when multiplied by phasor B_j at frequency ω_j, give contribution to the phasor C_i at frequency ω_i. The submatrix $Z^{(ij)}$ consists of three parts, corresponding to whether ω_i is the sum frequency, positive difference frequency or negative difference frequency of ω_k and ω_j

$$Z^{(ij)} = Z_p^{(k)} + Z_{mp}^{(k)} + Z_{mn}^{(k)}. \tag{19}$$

1) Sum frequency

$$Z_p^{(k)} = \begin{bmatrix} A_{kc} & -A_{ks} \\ A_{ks} & A_{ss} \end{bmatrix} \quad \omega_k + \omega_j = \omega_i \Rightarrow \omega_k = \omega_i - \omega_j. \tag{20a}$$

2) Positive difference frequency

$$Z_{mp}^{(k)} = \begin{bmatrix} A_{kc} & A_{ks} \\ A_{ks} & -A_{ss} \end{bmatrix} \quad \omega_k - \omega_j = \omega_i \Rightarrow \omega_k = \omega_i + \omega_j. \tag{20b}$$

3) Negative difference frequency

$$Z_{mn}^{(k)} = \begin{bmatrix} A_{kc} & A_{ks} \\ -A_{ks} & A_{ss} \end{bmatrix} \quad \omega_k - \omega_j = -\omega_i \Rightarrow \omega_k = \omega_j - \omega_i. \tag{20c}$$

Only those frequencies $\omega_k \in S$ are included in (20) which satisfy the condition

$$\mathrm{ORD}(\omega_k) + \mathrm{ORD}(\omega_j) \leq \mathit{maxIMp}. \tag{21}$$

Again, index tables are formed prior to the circuit analysis, corresponding to the three cases above. During the analysis, the construction of the matrix $\underline{\mathbf{A}}$ in (15) requires only assignment and addition operations on the elements of vector $\underline{\mathbf{a}}$. Vector $\underline{\mathbf{c}}$ is then obtained from the conventional matrix product.

Division: Calculating the convolution as a matrix product (15) with the help of the convolution matrix $\underline{\mathbf{A}} = \tilde{\mathbf{a}}$, has the consequence that the time-domain division (13) can be calculated by inverting this matrix

$$b(t) = c(t)/a(t) \;\Rightarrow\; \underline{\mathbf{b}} = \underline{\mathbf{A}}^{-1} \cdot \underline{\mathbf{c}}. \tag{22}$$

In practice $\underline{\mathbf{b}}$ is most efficiently calculated by solving the set of linear equations (22), explicit formulation of the inverse matrix is generally not required. Being able to calculate the division of two waveforms in the frequency domain allows us to use rational functions (and continued fractions) to model nonlinear components [12]. The same principle will also be used later to construct and invert the Jacobian in the Newton's method.

In this last application, the ability to control the order of intermodulation products in matrix $\underline{\mathbf{A}}$ by *maxIMp* is especially beneficial: in principle $\underline{\mathbf{A}}$ is a dense matrix, but reducing *maxIMp* results in sparser $\underline{\mathbf{A}}$, which additionally is then close to lower triangular. Fig. 3 shows an example of the structure of the convolution matrix. It is possible to take benefit from the sparsity and special structure of $\underline{\mathbf{A}}$ and write a special algorithm to solve the system (22) efficiently. In this work this has not yet been done, but $\underline{\mathbf{A}}$ is handled as a full matrix and Crout's algorithm is employed to solve the system of linear equations.

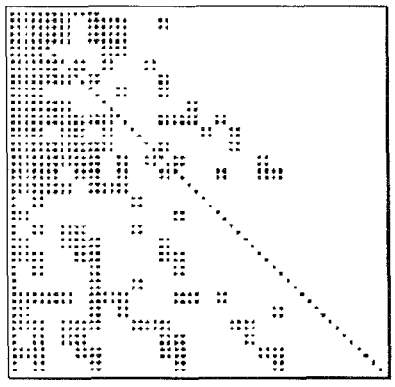

Fig. 3. Example of the structure of the convolution matrix. Each dot indicates a nonzero entry in the matrix. Two fundamental frequencies, *maxIMp* = 5.

III. Large-Signal Model

We now turn to the construction of the frequency-domain nonlinear model. The model is measurement based, which means that the measured small-signal data is used directly, without the need to fit the data to algebraic formulas. This work concentrates on the modeling of a MESFET, but the modeling principle is completely technology independent. In fact, this approach was used earlier in [9] to describe the currents of a "complete" black-box model for the extrinsic FET, including parasitics. In that work the separate determination of the parasitics was not necessary, they were included in the nonlinear model itself. Here we use the y-parameters of the intrinsic FET to construct the model; in this way the frequency-dependence of the y-parameters is less severe and lower order series are sufficient for the accurate representation of the y-parameters.

We assume that the currents at the two terminals of the intrinsic FET, driven with large-signal voltages $v_1(t), v_2(t)$, can be written in the following form $(i = 1, 2)$

$$\begin{aligned} i_i(t) &= g_i^{(0)}(v_1, v_2) + \frac{d}{dt} q_i^{(1)}(v_1, v_2) \\ &\quad + \frac{d^2}{dt^2} q_i^{(2)}(v_1, v_2) + \frac{d^3}{dt^3} q_i^{(3)}(v_1, v_2) + \cdots \\ &= g_i^{(0)}(v_1, v_2) + \dot{q}_i^{(1)}(v_1, v_2) + \ddot{q}_i^{(2)}(v_1, v_2) \\ &\quad + q_i^{(3)}(v_1, v_2) + \cdots. \end{aligned} \tag{23}$$

This expression is an extension of the conventional quasistatic formulation [14], [15], where only the first two terms of the series expansion are included, namely the static current through a nonlinear conductance, $g_i^{(0)}$, and the first order dynamic current through a nonlinear capacitance, $\dot{q}_i^{(1)}$. The higher order terms allow an accurate description of the frequency-dependence of the measured small-signal parameters, as will be shown below. We have a large-signal circuit model as shown in Fig. 4.

We require that the model is time-invariant, i.e., the nonlinear functions $g_i^{(0)}$ and $q_i^{(k)}$ are not explicit functions of time, but their time-dependence is solely through the dependence on the two controlling voltages. Further, we assume that the

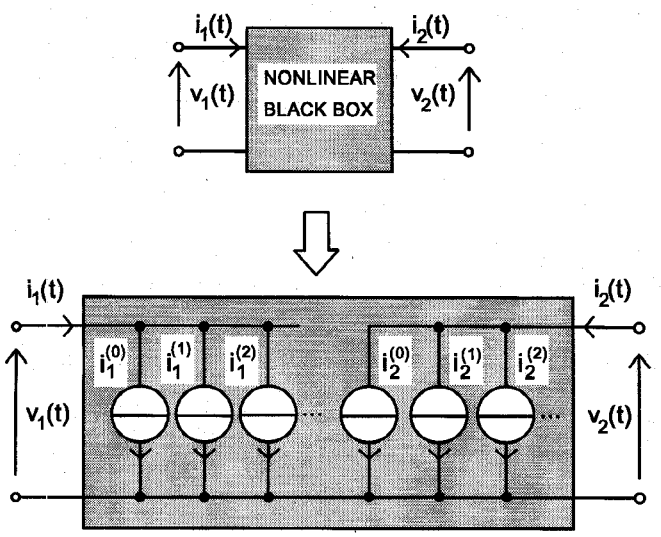

Fig. 4. Large-signal model for a nonlinear two-port.

partial derivatives of these functions

$$h_{ij}^{(0)}(v_1,v_2)=\frac{\partial g_i^{(0)}}{\partial v_j} \qquad h_{ij}^{(k)}(v_1,v_2)=\frac{\partial q_i^{(k)}}{\partial v_j}$$
$$i,j=1,2 \quad k=1,2,\cdots \tag{24}$$

depend only on the *instantaneous* voltages $v_1(t)$, $v_2(t)$, and not on their time-derivatives. With these assumptions, we can write the small-signal response of the device at port i, at dc bias point V_{10},V_{20}, to a small variation in the voltages $dv_1(t), dv_2(t)$in the following form

$$di_i(t)=h_{i1}^{(0)}dv_1+h_{i2}^{(0)}dv_2+h_{i1}^{(1)}d\dot{v}_1 + h_{i2}^{(1)}d\dot{v}_2+h_{i1}^{(2)}d\ddot{v}_1+h_{i2}^{(2)}d\ddot{v}_2+\cdots. \tag{25}$$

Here all the partial derivatives are developed at the dc operating point. Moving to the frequency domain, we obtain the response to a small sinusoidal excitation $dv_1(f_k), dv_2(f_k)$, at frequency f_k

$$di_i(f_k)=\left[h_{i1}^{(0)}+(j\omega_k)h_{i1}^{(1)}+(j\omega_k)^2h_{i1}^{(2)}+\cdots\right]\cdot dv_1(f_k) + \left[h_{i2}^{(0)}+(j\omega_k)h_{i2}^{(1)}+(j\omega_k)^2h_{i2}^{(2)}+\cdots\right]\cdot dv_2(f_k). \tag{26}$$

This can be compared with the measured small-signal response at a dc bias point (V_{10},V_{20})

$$di_i(f_k)=y_{i1}(V_{10},V_{20},\omega_k)\cdot dv_1(f_k) + y_{i2}(V_{10},V_{20},\omega_k)\cdot dv_2(f_k). \tag{27}$$

Here $y_{ij}(V_{10},V_{20},\omega_k)$ are the measured small-signal y-parameters of the intrinsic FET at the bias point (V_{10},V_{20}) and frequency f_k. We can now see that the higher order terms in (23) account for the frequency-dependence of the measured y-parameters: The second-order term gives quadratic frequency-dependence to the real part of y_{ij}, the third-order term causes cubic variation in the imaginary part of y_{ij} and so on. Thus we can identify each of the terms in (25) directly from the measurements. The large-signal functions in (23) can then be calculated from the path-independent line integrals [10]

$$g_i^{(0)}(v_1,v_2)=I_{i0}(V_{10},V_{20})+\int_{V_{10}}^{v_1(t)}h_{i1}^{(0)}(v_1,V_{20})dv_1 + \int_{V_{20}}^{v_2(t)}h_{i2}^{(0)}(v_1(t),v_2)dv_2 \tag{28a}$$

$$q_i^{(k)}(v_1,v_2)=\int_{V_{10}}^{v_1(t)}h_{i1}^{(k)}(v_1,V_{20})dv_1 + \int_{V_{20}}^{v_2(t)}h_{i2}^{(k)}(v_1(t),v_2)dv_2. \tag{28b}$$

We can notice that it is important that the small-signal functions $h_{ij}^{(k)}$ do not depend on the time-derivatives of the voltages, since, if this were the case, it would be impossible to construct the large-signal functions $g_i^{(0)}$ and $q_i^{(k)}$ from static small-signal measurements only. The model of (23) is quasistatic despite the presence of higher order terms in the series which correspond to higher order circuit elements [16] in the small-signal circuit model.

We observe that retaining only the first two terms in the series (23) gives resemblance to the Root model [10], where the frequency-dependence of the real parts of y_{11} and y_{12} (caused by the series connection of r_i with C_{gs} and r_{gd} with C_{gd}, respectively) are neglected. Keeping higher order terms in the series allows more accurate description of the frequency-dependence of the y-parameters of the intrinsic device in a consistent manner. The large-signal and small-signal models are inherently consistent, since the large-signal model is directly constructed from the small-signal characteristics through the line integrals (28). It should be noted that the "delay-effect," corresponding to the imaginary part of y_{21} (which is normally described with τ in small-signal models) is represented in this model with $h_{21}^{(1)}$, i.e., as a transcapacitance, as is done also in [10].

Next step in the modeling is finding the Chebyshev expansions to describe the dependence of each of the $h_{ij}^{(k)}$ functions on the two bias voltages. For example, for the static conductance we have

$$h_{ij}^{(0)}(v_1,v_2)=\sum_{n=0}^{L}\sum_{m=0}^{K}a_{mn}T_m(x)T_n(y). \tag{29}$$

Here x and y are the bias voltages, normalized to $[-1\cdots+1]$ and K and L are the degrees of the expansion in the two dimensions. Standard surface-fitting procedures can be used to determine the Chebyshev coefficients a_{mn} [17]. The coefficients are then written into matrix $\mathbf{H}_{ij}^{(0)}$, which has the dimension $(K+1)\times(L+1)$. In practice, the coefficients for a high-degree expansion are first determined and the degree is then reduced as long as the approximation error is acceptable. With the Chebyshev expansions, in contrast to the power series, the coefficients for a lower-degree expansion are found simply by truncation of the higher degree coefficients at the desired point.

For the evaluation of the line integrals in (28), the Chebyshev coefficients for the integrated small-signal functions have

to be determined. This is easily done from the coefficient matrices $\mathbf{H}_{ij}^{(k)}$ for the functions $h_{ij}^{(k)}$ by using the integration formula of the Chebyshev polynomials [18]. The resulting matrix of coefficients, integrated, e.g., over x (that is, over v_1), is written as $\mathbf{H}_{ijx}^{(k)}$.

IV. Evaluation of the Currents in the Frequency Domain

Functions approximated with Chebyshev expansion are evaluated in a numerically stabe manner by using the well-known Clenshaw's recurrence formula [18]. In the frequency domain, a two-dimensional function $f(x,y)$ is evaluated from the following recursion, by first calculating vectors $\mathbf{c}_i$ in y-direction for each $i = K,\ K-1, \cdots, 0$

$$\begin{aligned} \mathbf{b}_{L+2}^{(i)} &= \mathbf{b}_{L+1}^{(i)} = \mathbf{0} \\ \mathbf{b}_j^{(i)} &= 2 \cdot \mathbf{y} * \mathbf{b}_{j+1}^{(i)} - \mathbf{b}_{j+2}^{(i)} + a_{ij}\delta \quad j = L, L-1, \cdots, 0 \\ \mathbf{c}_i &= \frac{1}{2}\left(\mathbf{b}_0^{(i)} - \mathbf{b}_2^{(i)}\right). \end{aligned} \tag{30a}$$

Next, these coefficient vectors are used to evaluate the function in x-direction

$$\begin{aligned} \mathbf{d}_{K+2} &= \mathbf{d}_{K+1} = \mathbf{0} \\ \mathbf{d}_i &= 2 \cdot \mathbf{x} * \mathbf{d}_{i+1} - \mathbf{d}_{i+2} + \mathbf{c}_i \\ & \qquad i = K, K-1, \cdots, 0 \\ \mathbf{f}(\mathbf{x},\mathbf{y}) &= \frac{1}{2}(\mathbf{d}_0 - \mathbf{d}_2). \end{aligned} \tag{30b}$$

Here $\mathbf{x}$ and $\mathbf{y}$ are the normalized voltages $\mathbf{v}_1$ and $\mathbf{v}_2$, matrix $\mathbf{A}$ contains the Chebyshev coefficients a_{ij} and its dimension is $(K+1) \times (L+1)$ and $\boldsymbol{\delta}$ is a $(N+1) \times 1$ vector, with the first element equal to one and the others zeros. We use the short notation with operator $T\{\}$ for this recursion

$$\mathbf{f}(\mathbf{x},\mathbf{y}) = T\{\mathbf{A},\mathbf{x},\mathbf{y}\}. \tag{31}$$

We are now able to calculate the large-signal functions, given in (28), directly in the frequency domain, for given spectra of the driving voltages

$$\begin{aligned} \mathbf{g}_i(\mathbf{v_1},\mathbf{v_2}) &= T\{\mathbf{D}_i^{\mathrm{dc}}, x_0, y_0\}\boldsymbol{\delta} \\ &\quad + \alpha\cdot\left[T\left\{\mathbf{H}_{i1x}^{(0)},\mathbf{x},y_0\boldsymbol{\delta}\right\} - T\left\{\mathbf{H}_{i1x}^{(0)},x_0\boldsymbol{\delta},y_0\boldsymbol{\delta}\right\}\right] \\ &\quad + \beta\cdot\left[T\left\{\mathbf{H}_{i2y}^{(0)},\mathbf{x},\mathbf{y}\right\} - T\left\{\mathbf{H}_{i2y}^{(0)},\mathbf{x},y_0\boldsymbol{\delta}\right\}\right] \end{aligned} \tag{32a}$$

$$\begin{aligned} \mathbf{q}_i^{(k)}(\mathbf{v_1},\mathbf{v_2}) &= \alpha\cdot\left[T\left\{\mathbf{H}_{i1x}^{(k)},\mathbf{x},y_0\boldsymbol{\delta}\right\} - T\left\{\mathbf{H}_{i1x}^{(k)},x_0\boldsymbol{\delta},y_0\boldsymbol{\delta}\right\}\right] \\ &\quad + \beta\cdot\left[T\left\{\mathbf{H}_{i2y}^{(k)},\mathbf{x},\mathbf{y}\right\} - T\left\{\mathbf{H}_{i2y}^{(k)},\mathbf{x},y_0\boldsymbol{\delta}\right\}\right]. \end{aligned} \tag{32b}$$

Here x_0, y_0 is the normalized dc operating point, $\mathbf{D}_i^{\mathrm{dc}}$ is the matrix of Chebyshev coefficients for the dc current in port i and α and β account for the change of variables in the calculation of the line integrals

$$\begin{aligned} \alpha &= \frac{dv_1}{dx} = \frac{V_{1\max} - V_{1\min}}{2} \\ \beta &= \frac{dv_2}{dy} = \frac{V_{2\max} - V_{2\min}}{2}. \end{aligned} \tag{33}$$

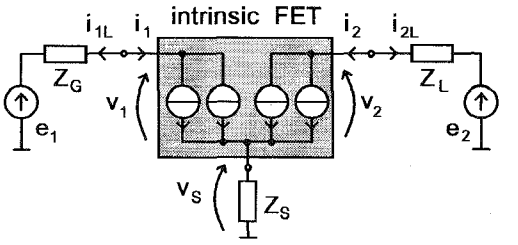

Fig. 5. Circuit model for the simulation of the mixer measurements.

The current at port i of the device, given in (23), is then calculated in the frequency domain

$$\begin{aligned} \mathbf{i}_i(\mathbf{v}_1,\mathbf{v}_2) &= \mathbf{g}_i(\mathbf{v}_1,\mathbf{v}_2) + \boldsymbol{\Omega}\cdot\mathbf{q}_i^{(1)}(\mathbf{v}_1,\mathbf{v}_2) \\ &\quad + \boldsymbol{\Omega}^2\cdot\mathbf{q}_i^{(2)}(\mathbf{v}_1,\mathbf{v}_2) + \cdots. \end{aligned} \tag{34}$$

Here $\boldsymbol{\Omega}$ is a $(N+1) \times (N+1)$ matrix with the angular frequencies $j\omega_k$in the diagonal and zero elsewhere.

V. Jacobian

The frequency-domain formulation of the analysis problem, presented in the preceding chapters, allows the construction of the Jacobian in a very economical way. We consider, as an example, the circuit of Fig. 5, which is used in the next chapter to analyse the operation of a MESFET as a mixer. The gate and drain currents of the intrinsic FET are represented with current sources, as was presented in the preceding chapter. Impedances Z_G, Z_L, and Z_S constitute the linear part of the circuit: Z_G includes the parasitics in series with the gate and the generator impedance, which is 50 Ω at RF frequencies. Similarly, Z_L represents parasitics at the drain lead and the load impedance. Voltage sources e_1 and e_2 provide the excitation to the circuit: e_1 includes the dc gate voltage, LO source and one or two RF generators, while e_2 consists only of the dc drain voltage.

Given the voltage spectra $\mathbf{v}_1$ and $\mathbf{v}_2$ at the terminals of the intrinsic FET, the gate and drain currents are calculated from (34), here written in an abbreviated form

$$\begin{cases} \mathbf{i}_1 = f_1(\mathbf{v}_1,\mathbf{v}_2) & \text{(35a)} \\ \mathbf{i}_2 = f_2(\mathbf{v}_1,\mathbf{v}_2)\,. & \text{(35b)} \end{cases}$$

The currents of the *linear* part of the circuit, calculated for the same voltages, are

$$\begin{cases} \mathbf{i}_{1L} = \mathbf{Y}_G\cdot(\mathbf{v}_1 + \mathbf{v}_S - \mathbf{e}_1) & \text{(36a)} \\ \mathbf{i}_{2L} = \mathbf{Y}_L\cdot(\mathbf{v}_2 + \mathbf{v}_S - \mathbf{e}_2)\,. & \text{(36b)} \end{cases}$$

Here $\mathbf{Y}_G$ and $\mathbf{Y}_L$ are diagonal matrices of the generator and load admittances. Ideally, the magnitudes of these currents should be the same as those calculated from the nonlinear part of the circuit in (35). However, since we do not not know exactly the correct voltages, we have the error vectors

$$\begin{cases} \boldsymbol{\varepsilon}_1 = \mathbf{i}_1 + \mathbf{i}_{1L} \\ \quad = [1 + \mathbf{Z}_S\cdot\mathbf{Y}_G]\cdot\mathbf{i}_1 \\ \quad\quad + \mathbf{Z}_S\cdot\mathbf{Y}_G\cdot\mathbf{i}_2 + \mathbf{Y}_G\cdot(\mathbf{v}_1 - \mathbf{e}_1) & \text{(37a)} \\ \boldsymbol{\varepsilon}_2 = \mathbf{i}_2 + \mathbf{i}_{2L} \\ \quad = \mathbf{Z}_S\cdot\mathbf{Y}_L\cdot\mathbf{i}_1 + [1 + \mathbf{Z}_S\cdot\mathbf{Y}_L]\cdot\mathbf{i}_2 \\ \quad\quad + \mathbf{Y}_L\cdot(\mathbf{v}_2 - \mathbf{e}_2)\,. & \text{(37b)} \end{cases}$$

Here 1 is the identity matrix with dimension (*Nfreq* × *Nfreq*). For the next iteration, we have to find the changes in the voltages, $\Delta\mathbf{v}_1$ and $\Delta\mathbf{v}_2$, that are needed to reduce the predicted error to zero. In the time domain, changes $\Delta v_1(t), \Delta v_2(t)$ cause the following changes in the currents

$$\begin{cases} \Delta i_1(t) = \frac{\partial i_1}{\partial v_1} \cdot \Delta v_1(t) + \frac{\partial i_1}{\partial v_2} \cdot \Delta v_2(t) & \text{(38a)} \\ \Delta i_2(t) = \frac{\partial i_2}{\partial v_1} \cdot \Delta v_1(t) + \frac{\partial i_2}{\partial v_2} \cdot \Delta v_2(t)\ . & \text{(38b)} \end{cases}$$

Writing the spectra of the derivative waveforms as $\mathbf{h}_{ij}$, the changes in the frequency domain can be written with the help of convolutions

$$\begin{cases} \Delta\mathbf{i}_1 = \mathbf{h}_{11} * \Delta\mathbf{v}_1 + \mathbf{h}_{12} * \Delta\mathbf{v}_2 & \text{(39a)} \\ \Delta\mathbf{i}_2 = \mathbf{h}_{21} * \Delta\mathbf{v}_1 + \mathbf{h}_{22} * \Delta\mathbf{v}_2\ . & \text{(39b)} \end{cases}$$

Each term $\mathbf{h}_{ij}$ consists of zeroth and higher order terms, up to the desired level

$$\mathbf{h}_{ij} = \mathbf{h}_{ij}^{(0)} + \Omega \cdot \mathbf{h}_{ij}^{(1)} + \Omega^2 \cdot \mathbf{h}_{ij}^{(2)} + \cdots . \qquad \text{(40)}$$

Calculating the convolutions from matrix products, as in (15), we get

$$\begin{cases} \underline{\Delta\mathbf{i}}_1 = \tilde{\underline{\mathbf{h}}}_{11} \cdot \underline{\Delta\mathbf{v}}_1 + \tilde{\underline{\mathbf{h}}}_{12} \cdot \underline{\Delta\mathbf{v}}_2 & \text{(41a)} \\ \underline{\Delta\mathbf{i}}_2 = \tilde{\underline{\mathbf{h}}}_{21} \cdot \underline{\Delta\mathbf{v}}_1 + \tilde{\underline{\mathbf{h}}}_{22} \cdot \underline{\Delta\mathbf{v}}_2\ . & \text{(41b)} \end{cases}$$

Underlining here, as before, indicates that in the corresponding vectors and matrices the real and imaginary parts are written as real numbers, instead of the normal representation with complex numbers. We can now write the resulting change in the error vectors from (37). The corrections to the voltages for the next iteration $\Delta\mathbf{v}_1, \Delta\mathbf{v}_2$ are obtained by requiring that this change cancels the error vectors of the current iteration as shown in (42) at the bottom of the page. The matrix on the right-hand side is the Jacobian $\underline{\mathbf{J}}$. By combining the error and voltage vectors into single vectors ϵ and $\Delta\mathbf{v}$, the correction to the voltages is calculated by solving the set of equations

$$\underline{\Delta\mathbf{v}} = \underline{\mathbf{J}}^{-1} \cdot (-\underline{\epsilon}). \qquad \text{(43)}$$

This way of constructing the Jacobian is remarkably simple and part of the calculations needed are in fact already done when evaluating the currents from (32) and can be simply reused here. The transformation "$\sim$" in (41) is very fast, since precalcuated index vectors are used, as was discussed earlier. Overall, in all the cases considered up to now, the additional computer time required for construction and inverting the Jacobian has been shorter than the time required for the actual evaluation of the nonlinear functions.

VI. Model for a MESFET

A large-signal model was constructed for a 1 × 300 μm monolithic MESFET ($V_T = -1.5$ V) using the principle described above. First, dc measurements were made and then s-parameters were measured (on wafer) over the entire operating range of bias voltages (161 bias points, $V_{gs} = -3 \cdots 0.75$ V, $V_{ds} = 0 \cdots 5$ V) and frequencies ($0.1 \cdots 18.1$ GHz). Parasitics were extracted with the help of the measurements on cold FET and Chebyshev expansions were fitted on the y-parameters of the intrinsic FET.

In order to get an impression of how well the bias-dependent small-signal model, consisting of Chebyshev polynomials, represents the measured frequency and bias characteristics of the FET, s-parameters of the model, including the parasitics, were calculated at each bias point over the entire frequency range from 0.82 to 18.1 GHz. At each point $m = 1, \cdots, 2737$ (161 bias points ×17 frequencies = 2737 points in total) an error vector $\Delta s_{ij}(m)$ was calculated from the measured $(s_{ij}(m))$ and from the model calculated $(s'_{ij}(m))$ s-parameters

$$\Delta s_{ij}(m) = s_{ij}(m) - s'_{ij}(m) \qquad i,j = 1,2 \quad m = 1,2,\cdots,2737. \qquad \text{(44)}$$

The following statistical quantities were then calculated for each s-parameter.

- ABS.ERR average magnitude of the error vector. $|\Delta s_{ij}(m)|$.
- MAX.ERR maximum absolute error $|\Delta s_{ij}(m)|$.
- STD.DEV standard deviation of $|\Delta s_{ij}(m)|$.
- REL.ERR average relative error $|\Delta s_{ij}(m)|/|s_{ij}(m)|$.

The effect of including higher order terms in (26) was first studied. The first entry in Table I, marked with (a), shows the statistics of the approximation errror with terms up to order 5 included in the series. Each y-parameter was approximated with a double Chebyshev expansion with the maximum degree $K = L = 12$ which is sufficiently high to accurately describe the bias-dependence of the y-parameters in most bias points. Taking into account the very wide bias range (from far below cutoff to strong gate conduction), the average errors are very small, with typically 3% approximation error in the s-parameters. The maximum errors are greater, mainly due to the fact that the maximum degree of 12 is not sufficient to accurately represent the exponential nonlinearity of the gate junction.

The next lines in Table I, marked with (b), show the error statistics when only the static and first order dynamic elements are included in the series describing the frequency-dependence of the y-parameters, i.e., the admittances of the intrinsic FET are modeled with a parallel connection of a nonlinear capacitance and conductance, as is done in the Root model [10]. Again the degree of the Chebyshev expansions

$$\begin{bmatrix} -\underline{\epsilon}_2 \\ -\underline{\epsilon}_2 \end{bmatrix} = \begin{bmatrix} [1 + \underline{\mathbf{Z}}_S \cdot \underline{\mathbf{Y}}_G] \cdot \tilde{\underline{\mathbf{h}}}_{11} + \underline{\mathbf{Z}}_S \cdot \underline{\mathbf{Y}}_G \cdot \tilde{\underline{\mathbf{h}}}_{21} + \underline{\mathbf{Y}}_G & [1 + \underline{\mathbf{Z}}_S \cdot \underline{\mathbf{Y}}_G] \cdot \tilde{\underline{\mathbf{h}}}_{12} + \underline{\mathbf{Z}}_S \cdot \underline{\mathbf{Y}}_G \cdot \tilde{\underline{\mathbf{h}}}_{22} \\ [1 + \underline{\mathbf{Z}}_S \cdot \underline{\mathbf{Y}}_L] \cdot \tilde{\underline{\mathbf{h}}}_{21} + \underline{\mathbf{Z}}_S \cdot \underline{\mathbf{Y}}_L \cdot \tilde{\underline{\mathbf{h}}}_{11} & [1 + \underline{\mathbf{Z}}_S \cdot \underline{\mathbf{Y}}_L] \cdot \tilde{\underline{\mathbf{h}}}_{22} + \underline{\mathbf{Z}}_S \cdot \underline{\mathbf{Y}}_L \cdot \tilde{\underline{\mathbf{h}}}_{12} + \underline{\mathbf{Y}}_L \end{bmatrix} \cdot \begin{bmatrix} \underline{\Delta\mathbf{v}}_1 \\ \underline{\Delta\mathbf{v}}_2 \end{bmatrix} \qquad \text{(42)}$$

TABLE I
STATISTICS OF THE SMALL-SIGNAL MODELING ERROR IN DIFFERENT CASES: (a) WITH HIGH ORDER ELEMENTS UP TO ORDER 5 INCLUDED, (b) WITH ONLY ZEROTH AND FIRST ORDER ELEMENTS INCLUDED, AND (c) SAME AS CASE (b) BUT USING TRUNCATED CHEBYSHEV EXPANSIONS

		s_{11}	s_{12}	s_{21}	s_{22}
ABS.ERR	(a)	0.011	0.004	0.027	0.015
	(b)	0.039	0.012	0.097	0.040
	(c)	0.038	0.013	0.097	0.037
MAX.ERR	(a)	0.254	0.057	0.198	0.108
	(b)	0.269	0.067	0.233	0.117
	(c)	0.201	0.053	0.553	0.134
STD.DEV	(a)	0.020	0.005	0.024	0.013
	(b)	0.023	0.008	0.047	0.014
	(c)	0.027	0.010	0.083	0.024
REL.ERR	(a)	0.013	0.026	0.036	0.028
	(b)	0.036	0.052	0.094	0.054
	(c)	0.054	0.068	0.124	0.064

is 12. We can see that, while the errors are still small, the average errors have increased by a factor of two to three due to the frequency-dependence of the real and imaginary parts of the intrinsic y-parameters. This is also demonstrated in Fig. 6 which shows the measured and modeled s-parameters at a single bias point. In Fig. 6(a) all the higher order elements up to order 5 are present and in Fig. 6(b) the model consists only of the zeroth and first order elements. It is apparent that the simple model with only parallel nonlinear RC elements is sufficient at lower frequencies (below 6 GHz), while it cannot accurately model the variation of s_{11}, s_{21} and s_{22} at higher frequencies.

Since the mixer measurements of the next chapter were performed at low frequencies with RF and LO around 1 GHz, the simple model without higher order elements was considered sufficient. This also helps in minimizing the computer time which is an important factor in mixer intermodulation analysis where the calculations tend to be very time-consuming. For example, the model used in Fig. 6(a) with up to fifth-order elements requires three times as many convolution operations as the simple model used in Fig. 6(b). The adopted simple model can be drawn as in Fig. 7, where the y-parameters of the intrinsic FET are represented with the branch admittances, each consisting of a parallel connection of a nonlinear conductance and a nonlinear capacitance. This way of presenting the large-signal model is not necessarily required, the measured y-parameters could be handled directly. However, this circuit representation is widely used and the circuit elements can be readily associated with physical characteristics of the device.

Using high-degree Chebyshev expansions in the circuit analysis would be wasteful since comparable accuracy can be obtained with lower degree expansions with much less computations. Consequently the next step is to decrease the degree of the Chebyshev expansions as much as possible

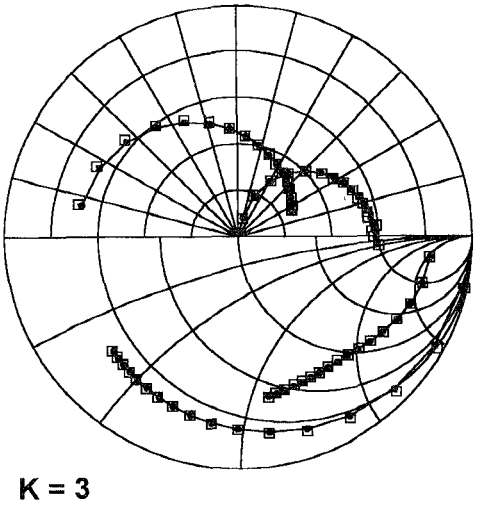

(a)

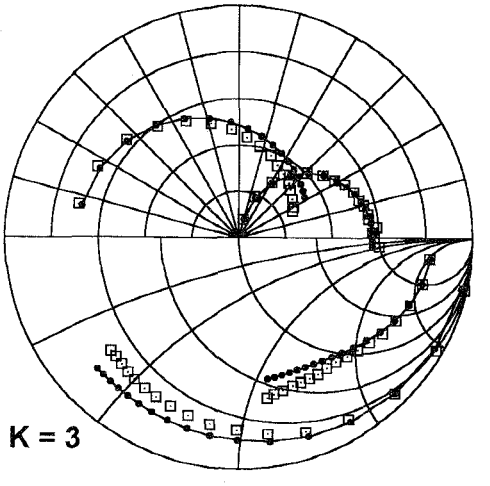

(b)

Fig. 6. Effect of the higher order elements in the model with measured (squares) and modeled (dots) s-parameters 1 to 18 GHz. In (a) orders up to 5 are included. In (b) only the zeroth (= conductance) and first order (= capacitance) elements are included. $V_{gs} = -1.0$ V and $V_{ds} = 2.5$ V.

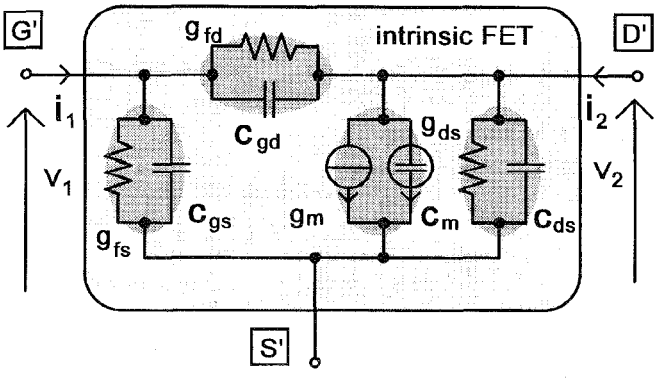

Fig. 7. Small-signal circuit model for the intrinsic FET used in the mixer simulations.

while keeping the approximation error acceptable. After some experimentation it was found that the values in Table II give

TABLE II
SELECTED DEGREES OF CHEBYSHEV EXPANSIONS

I_g, g_{fs}	$K=28$	
g_{fd}	$K=46$	
I_d, g_m, g_{ds}	$K=8$	$L=8$
C_{gs}, C_{gd}, C_m, C_{ds}	$K=6$	$L=6$

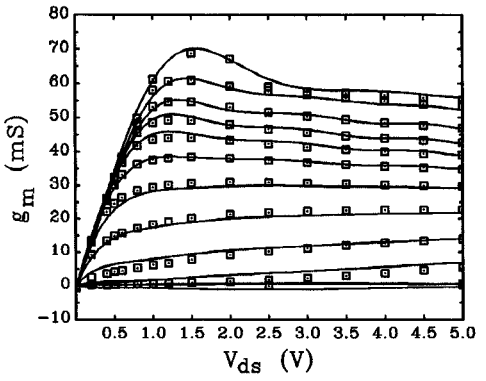

Fig. 8. From the measurements extracted (squares) and with the Chebyshev expansions modeled (lines) dependence of the transconductance on the bias voltages.

an acceptable approximation error. Those elements which describe the gate conduction (I_g, g_{fs}, g_{fd}), require large number of terms in the Chebyshev series. However, since they are mainly controlled by a single voltage (v_1 and $v_1 - v_2$), single Chebyshev expansions were used to describe them. In fact, it was found that the most difficult term, g_{fd}, is not required at drain voltages $v_2 > 0.3$ V. In the calculations of this work this was always the case and consequently g_{fd} was left out of the model. Again the s-parameters of the model were calculated at each of the 2737 points and compared to the measured s-parameters. The results are shown on the lines marked with (c) in Table I. The accuracy of the approximation can be visualised from Fig. 8 which shows, as an example, the bias-dependence of the transconductance, as obtained from the measurements and from the model with truncated Chebyshev series.

Thus we have arrived at the coefficient matrices $\mathbf{H}_{ij}^{(k)}$ for each of the elements in the small-signal bias-dependent model. The large-signal currents are calculated from the line integrals (28) and we have to determine the coefficient matrices integrated over one of the controlling voltages, e.g., $\mathbf{H}_{ij,v}^{(k)}$. In principle, the line integrals should be independent of the integration path. However, the small-signal functions are generated from measurements through truncation of the Chebyshev expansions and therefore always contain some amount of error with the result that the condition of integrability is not exactly met. In order to get an impression of the magnitude of this problem, a test case was analysed with the FET driven with a moderately strong signal (+3 dBm) using two different paths of integration. The current waveforms were found to be almost identical, the main difference between the two integration paths was a small difference in the dc drain current. This gives an indication that the condition of integrability was quite closely met. However, this question certainly requires further investigation in the future.

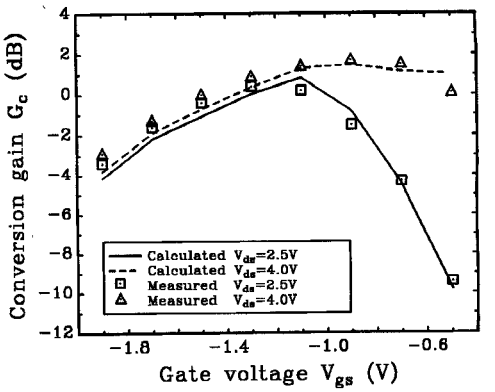

(a)

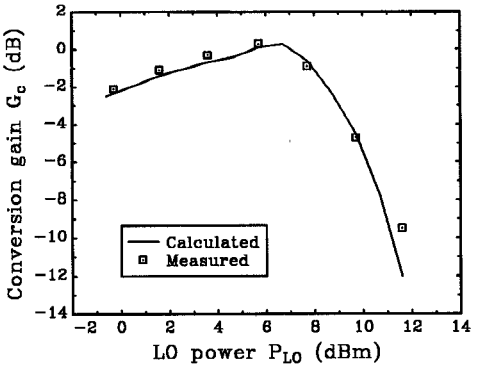

(b)

Fig. 9. Comparison of the measured (symbols) and simulated (lines) conversion gain of the mixer. (a) Shows the dependence on the bias voltages, and (b) shows the effect of the local oscillator power.

VII. MEASURED AND CALCULATED RESULTS

The constructed large-signal model was then used to simulate mixer measurements which were made on wafer using the same FET chip, with both the drain and source terminated to 50 Ω. The effect of the bias voltages and local oscillator (LO) power on the conversion gain ($f_{\mathrm{RF}} = 0.8$ GHz, $f_{\mathrm{LO}} = 0.9$ GHz) were measured around the experimentally found best operating point $V_{\mathrm{gs}} = -1.3$ V, $P_{\mathrm{LO}} = 6$ dBm at drain voltage $V_{\mathrm{ds}} = 2.5$ V. These measurements were simulated with the frequency-domain algorithm with three harmonics of RF, five harmonics of LO and intermodulation products up to order five taken into account, or with 27 frequencies in total. Fig. 9 shows both the measured and simulated results. We can see that the effects of bias voltages and LO power are accurately predicted by the simulation.

Finally, mixer intermodulation measurements were made at the same operating point by sweeping the power level of two closely (5 MHz) separated RF tones and observing the power levels of the IF and third-order intermodulation products on spectrum analyzer. Again, the measurement was simulated using the frequency-domain method. Three harmonics of the

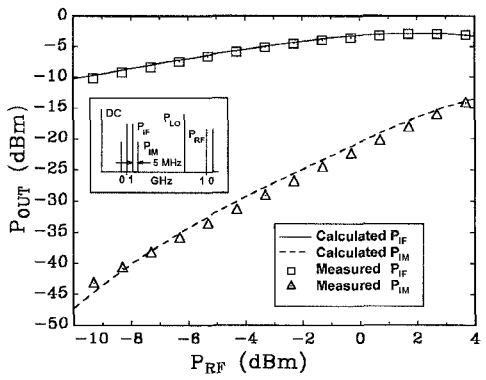

Fig. 10 Measured (symbols) and simulated (lines) IF and IM levels at the output of the mixer.

two RF signals, five harmonics of the LO and intermodulation products up to order five, or 104 frequencies in total, were taken into account. In order to be able to extend the simulation to relatively high power levels, i.e., past saturation of the IF, it was necessary to widen the normalization range of the gate voltage to $-5 \cdots 0.8$ V by extrapolation. Measured and simulated results are shown in Fig. 10, and again we can notice excellent agreement. The computer used in all the calculations was a 486 machine with 8 Mbyte RAM.

VIII. Conclusion

An analysis method has been presented that extends the applicability of the frequency-domain methods to strongly nonlinear circuits. This was made possible by the use of Chebyshev expansions to describe the nonlinear functions. Nonlinear functions are evaluated directly in the frequency domain with the three-term recurrence formula of orthogonal polynomials. This procedure is numerically stable so that high-degree expansions can be employed to describe strongly nonlinear functions.

A novel frequency-domain modeling scheme for nonlinear devices has been developed. The model is inherently self-consistent due to the measurement-based construction: The large-signal currents are directly constructed from small-signal y-parameters through contour integration. The model has the advantage that the frequency-dependence of measured small-signal parameters can be described as accurately as desired. The model consists of polynomials, therefore, all the derivatives of interest exist and are continuous. Frequency-domain construction guarantees inherent accuracy in describing frequency-dependent characteristics, like g_{ds}, of the nonlinear devices.

The analysis method and modeling approach have been experimentally verified through excellent correspondence of the measured and simulated results on a monolithic MESFET operating as mixer. The efficiency of the frequency-domain method has been demonstrated by analysing the intermodulation distortion of the mixer with three independent tones and over 100 frequencies in total, driven past saturation with strong RF signals, on a personal computer.

References

[1] S A. Maas and D. A. Neilson, "Modeling MESFET's for intermodulation analysis of mixers and amplifiers," *IEEE Trans. Microwave Theory Tech.*, vol 38, no 12, pp 1964–1971, Dec 1990.

[2] V. Rizzoli, C Cecchetti, A Lipparini, and F Mastri, "General-purpose harmonic balance analysis of nonlinear microwave circuits under multitone excitation," *IEEE Trans Microwave Theory Tech*, vol. 36, pp 1650–1659, Dec. 1988.

[3] M. B. Steer, C.-R. Chang, and G. W. Rhyne, "Computer-aided analysis of nonlinear microwave circuits using frequency-domain nonlinear analysis techniques: The state of the art," *Int. J. Microwave Millimeter-Wave Computer-Aided Engineering*, vol. 1, no. 2, pp. 181–200, 1991.

[4] G. W. Rhyne, M. B. Steer, and B. D. Bates, "Frequency-domain nonlinear circuit analysis using generalized power series," *IEEE Trans. Microwave Theory Techn*, vol. 36, no 2, pp 379–387, Feb. 1988

[5] T. Närhi, "Multi-frequency analysis of nonlinear circuits using one- and two-dimensional series expansions," in *Proc 19th European Microwave Conf*, Sept. 1989, pp. 375–379.

[6] C.-R. Chang and M. B. Steer, "Frequency-domain nonlinear microwave circuit simulation using the arithmetic operator method," *IEEE Trans Microwave Theory Tech.*, vol. 38, no. 8, pp. 1139–1143, Aug 1990.

[7] T. Narhi, "Frequency-domain analysis of nonlinear microwave circuits," Dr.Tech. thesis, VTT Publications 148, Technical Research Centre of Finland, Espoo, Finland, 1993.

[8] T. Närhi, "Analysis of strongly nonlinear circuits with a frequency-domain method coupled with a consistent large-signal model," in *IEEE MTT-S Int Microwave Symp Dig.*, 1993, pp. 633–636

[9] T. Narhi, "Black-box modeling of nonlinear devices for frequency-domain analysis," in *Proc. 22th European Microwave Conf*, Aug. 1992, pp. 1109–1114.

[10] D. E. Root, S. Fan, and J. Meyer, "Technology independent large-signal nonquasistatic FET models by direct construction from automatically characterized device data," in *Proc. 21st European Microwave Conf.*, Sept. 1991, pp. 927–932.

[11] J. E Dennis and R. B. Schnabel, *Numerical Methods for Unconstrained Optimization and Nonlinear Equations*. Englewood Cliffs, NJ: Prentice-Hall, 1983.

[12] T. Närhi, "Frequency domain modeling of strongly nonlinear components," in *Proc 3rd Asia-Pacific Microwave Conf.*, Tokyo, Sept. 18–21, 1990, pp. 325–328

[13] C.-R. Chang, M. B. Steer, and G. W. Rhyne, "Frequency-domain spectral balance using the arithmetic operator method," *IEEE Trans. Microwave Theory Tech.*, vol. 37, no. 11, pp. 1681–1688, Nov. 1989.

[14] K S. Kundert and A Sangiovanni-Vincentelli, "Simulation of nonlinear circuits in the frequency domain," *IEEE Trans. Computer-Aided Design*, vol. CAD-5, pp. 521–535, Oct. 1986

[15] D E. Root, S. Fan and J. Meyer, "Technology-independent large-signal FET models: A measurement based approach to active device modeling," in *Proc 15th ARMMS Conf.*, Sept 1991

[16] L. O. Chua, "Device modeling via basic nonlinear circuit elements," *IEEE Trans. Circuits Syst*, vol. CAS-27, no. 11, pp 1014–1044, Nov 1980.

[17] C W Clenshaw and J. G. Hayes, "Curve and surface fitting," *J. Inst. Maths Applicat.*, vol. 1, pp. 164–183, 1965.

[18] L. Fox and I. B. Parker, *Chebyshev Polynomials in Numerical Analysis*. London: Oxford Univ Press, 1968.

Tapani Närhi, photograph and biography not available at the time of publication.